# Reactions of Zirconium and Hafnium Atoms with Ammonia. Matrix Infrared Spectra and Density Functional Calculations of the $MNH_3$ and $H_2MNH$ (M = Zr and Hf) Molecules

**Mingfei Zhou,* Mohua Chen, Luning Zhang, and Hao Lu**

*Department of Chemistry and Laser Chemistry Institute, Fudan University, Shanghai 200433, P.R. China*

*Received: April 12, 2002; In Final Form: June 10, 2002*

The reactions between zirconium and hafnium metal atoms and ammonia molecules have been studied using matrix isolation infrared absorption spectroscopy and density functional theoretical calculations. The results showed that ground-state zirconium and hafnium metal atoms reacted with $NH_3$ to form the $ZrNH_3$ and $HfNH_3$ complexes spontaneously on annealing. The $ZrNH_3$ and $HfNH_3$ complexes underwent photochemical rearrangement to the $HZrNH_2$, $H_2ZrNH$, and $H_2HfNH$ molecules. The reaction intermediates and products have been identified by isotopic substitutions as well as density functional theoretical frequency calculations. In addition, qualitative analysis of the possible reaction paths for these reactions is given, including various minima and transition states.

## Introduction

The oxidative addition of the N−H bond of ammonia or amines to transition metal centers is an important reaction in many catalytic processes.[1] The interaction of transition metal cations with ammonia molecules has attracted considerable attention during the past 2 decades.[2−15] It has been shown that the reactions of early transition metal cations $Sc^+$, $Ti^+$, and $V^+$ with ammonia led to the formation of $ScNH^+$, $TiNH^+$, and $VNH^+$ as dominate product at low energies.[2−4] The production of $MNH^+$ has been proposed to proceed via the facile formation of a $MNH_3^+$ complex followed by oxidative addition to form an insertion intermediate $HMNH_2^+$.[5,8,9] In the reactions of cobalt cation, a long-lived insertion product $HCo^+NH_2$ has been observed.[10]

Laser-ablated scandium atoms reacted with ammonia in the gas phase to form ScNH, which was detected and characterized by laser-induced fluorescence spectroscopy.[16] Recent gas-phase studies indicated that ground state yttrium atoms readily react with ammonia to form YNH.[17] There are also a few examples of the insertion of a transition metal atom into the N−H bond of an ammonia molecule.[18−21] In solid matrixes, Fe, Ni, and Cu atoms formed adduct with one or two $NH_3$ molecules, and UV irradiation induced the insertion of the metal into a N−H bond of $NH_3$ with the formation of the amido derivatives $HMNH_2$ (M = Fe, Ni, and Cu), $HMNH_2NH_3$ (M = Fe or Ni), and $MNH_2$ (M = Cu).[18−20] Recently, reactions between early transition metal atoms (Sc, Ti, and V) and ammonia have been investigated in this laboratory.[21] Our results showed that ground-state Sc, Ti, and V atoms reacted with ammonia in solid argon matrix to form the $MNH_3$ complexes spontaneously on annealing. Photoisomerism to form the insertion intermediate $HMNH_2$, the imide ScNH, and the novel covalently bounded $H_2MNH$ (M = Ti and V) molecules proceeded upon different UV−visible photolyses.

The interaction of transition metal atoms with ammonia has also attracted several quantum chemical calculations. The geometries, vibrational properties, energetics, and the nature of bonding of transition metal atom−ammonia complexes have been reported.[22−27] The oxidative addition reactions between ammonia and the second row transition metal atoms have been theoretically investigated.[28] Geometries and energies for molecular adducts, transition states, and insertion products have been obtained. The lowest barriers for the N−H insertion reaction were found for the early transition metal atoms with values slightly below zero.

In the present study, we report a combined matrix isolation infrared spectroscopic and theoretical investigation of the reactions between zirconium and hafnium atoms and ammonia molecules.

## Experimental and Computational Methods

The experimental setup for pulsed laser ablation and matrix infrared spectroscopic investigation has been described previously.[29] Briefly, the 1064 nm Nd:YAG laser fundamental (Spectra Physics, DCR 150, 20 Hz repetition rate and 8 ns pulse width) was focused onto the rotating zirconium or hafnium metal target, and the ablated metal atoms were codeposited with ammonia in excess argon onto a 11 K CsI window, which was mounted on a cold tip of a closed-cycle helium refrigerator (Air Products, Model CSW202) for 1 h at a rate of around 5 mmol/h. Typically, 5−20 mJ/pulse laser power was used. Infrared spectra were recorded on a Bruker IFS113V spectrometer at 0.5 $cm^{-1}$ resolution using a DTGS detector. Isotopic $^{15}NH_3$ was prepared by thermal dissociation of $(^{15}NH_4)_2SO_4$ (98%). Mixed $NH_3 + NH_2D + NHD_2 + ND_3$ was obtained by thermal dissociation of partially deuterated $(NH_3)_2SO_4$ prepared through exchange by $D_2O$. Matrix samples were annealed at different temperatures and subjected to different wavelength photolyses using a high-pressure mercury lamp (250 W, without globe) and glass filters.

Quantum chemical calculations were performed using the Gaussian 98 program.[30] The Becke's three parameter hybrid functional with the Lee, Yang, and Parr correlation corrections was utilized (B3LYP).[31] The 6-311++G(d,p) basis sets were used for H and O atoms, and the Los Alamos ECP plus DZ (LANL2DZ) sets were used on Zr and Hf atoms.[32] These ECPs

* Corresponding author. Fax:+86-21-65643532. E-mail: mfzhou@fudan.edu.cn.

10.1021/jp020971w CCC: $22.00 
Published on Web 09/07/2002

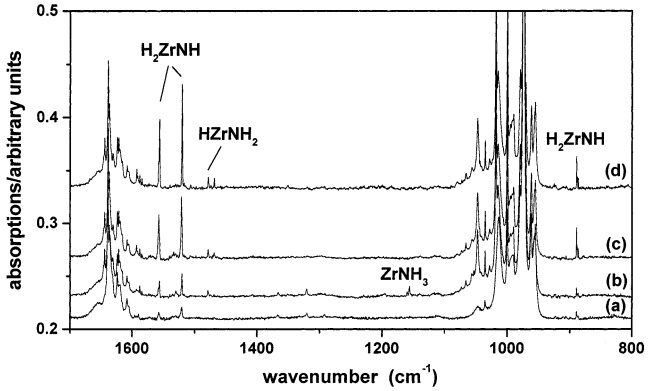


**Figure 1.** Infrared spectra in the 1660−800 $cm^{-1}$ region from codeposition of laser-ablated zirconium atoms with 0.2% $NH_3$ in argon: (a) 1 h sample deposition at 11 K, (b) after 25 K annealing, (c) after 20 min broadband photolysis, and (d) after 28 K annealing.

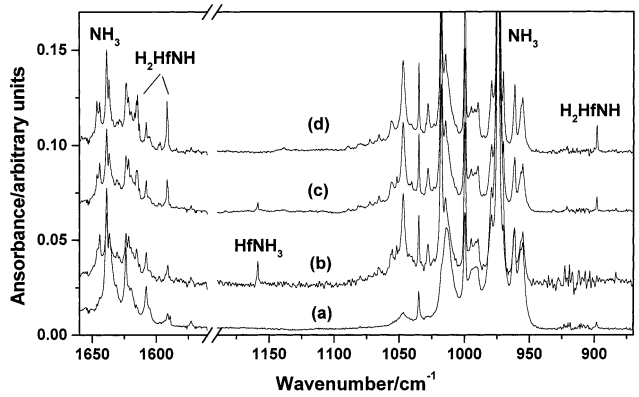


**Figure 2.** Infrared spectra in the 1660−1560 and 1190−870 $cm^{-1}$ regions from codeposition of laser-ablated hafnium atoms with 0.2% $NH_3$ in argon: (a) 1 h sample deposition at 11 K, (b) after 25 K annealing, 20 scans, (c) after 25 K annealing, 200 scans, and (d) after 20 min broadband photolysis.

have incorporated Darwin relativistic effects into the potentials. Recent studies have shown that density functional theory using this hybrid functional and effective core potentials can provide quite reliable predictions of the state energies, structures, and vibrational frequencies of second and third row transition metal containing compounds.[33] Reactants, various possible transition states, intermediates, and products were optimized. The vibrational frequencies were calculated with analytic second derivatives, and zero point vibrational energies (ZPVE) were derived. Transition state optimizations were done with the synchronous transit-guided quasi-Newton (STQN) method,[34] followed by the vibrational frequency calculations showing the obtained structures to be true saddle points.

## Results and Discussions

**Infrared Spectra.** Reactions of laser-ablated zirconium and hafnium atoms with ammonia were examined with a range of laser energies, ammonia concentrations, and isotopic modifications. Infrared spectra in selected regions for the products of zirconium and hafnium atoms reacting with ammonia in excess argon are presented in Figures 1 and 2. The product absorptions are listed in Table 1. Absorptions due to $NH_3$ ($\nu_2$, 974.7 $cm^{-1}$; $\nu_4$, 1638.8 $cm^{-1}$), $(NH_3)_n$ ($n = 2$, 999.9, 1631.0 $cm^{-1}$; $n = 3$, 1018.0 $cm^{-1}$), and a trace of water ($\nu_2$, 1624.0, 1608.1, and 1589.2 $cm^{-1}$), which are common to experiments with $NH_3$ and transition metals, are omitted from the table.[35] The stepwise annealing and photolysis behavior of the product absorptions

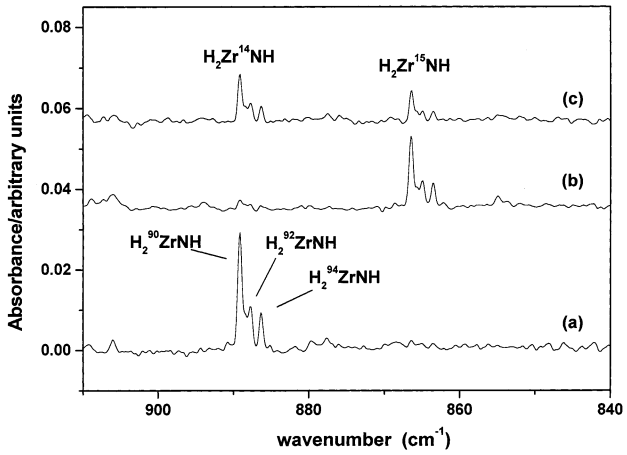


**Figure 3.** Infrared spectra in the 910−840 $cm^{-1}$ region from codeposition of laser-ablated zirconium atoms with $NH_3$ in excess argon: (a) 0.2% $^{14}NH_3$, after 20 min broadband photolysis, (b) 0.2% $^{15}NH_3$, after 20 min broadband photolysis, and (c) 0.12% $^{14}NH_3$ + 0.08% $^{15}NH_3$, after 20 min broadband photolysis.

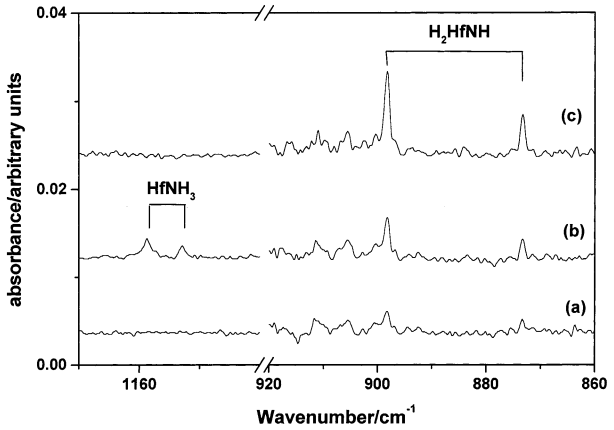


**Figure 4.** Infrared spectra in the 1170−1120 and 920−860 $cm^{-1}$ regions from codeposition of laser-ablated hafnium atoms with 0.12% $^{14}NH_3$ + 0.08% $^{15}NH_3$ in argon: (a) 1 h sample deposition at 11 K, (b) after 25 K annealing, and (c) after 20 min broadband photolysis.

**TABLE 1: Infrared Absorptions ($cm^{-1}$) from Codeposition of Laser-Ablated Zr and Hf Atoms with Ammonia in Excess Argon**

| $^{14}NH_3$ | $^{15}NH_3$ | $ND_3$ | assignment |
|---|---|---|---|
| 1556.0 | 1556.0 | 1114.9 | $H_2ZrNH$, $\nu_{sym}(ZrH_2)$ |
| 1520.3 | 1520.2 | 1094.7 | $H_2ZrNH$, $\nu_{asym}(ZrH_2)$ |
| 1478.4 | 1478.4 | 1056.9 | $HZrNH_2$, $\nu$(Zr−H) |
| 1156.0 | 1149.4 | | $ZrNH_3$, $\delta_{sym}(NH_3)$ |
| 889.2 | 866.5 | | $H_2{}^{90}ZrNH$, $\nu$(Zr−NH) |
| 887.8 | 865.0 | | $H_2{}^{92}ZrNH$ |
| 886.4 | 863.5 | | $H_2{}^{94}ZrNH$ |
| 1614.7 | 1614.7 | 1160.7 | $H_2HfNH$, $\nu_{sym}(HfH_2)$ |
| 1590.9 | 1590.9 | 1140.7 | $H_2HfNH$, $\nu_{asym}(HfH_2)$ |
| 1158.8 | 1152.9 | | $HfNH_3$, $\delta_{sym}(NH_3)$ |
| 898.3 | 873.2 | | $H_2HfNH$, $\nu$(Hf−NH) |

is also shown in the figures and will be discussed below. Nitrogen-15- and deuterium-substitution experiments were also employed for product identification through isotopic shift and splitting. Typical spectra using $^{14}NH_3$ + $^{15}NH_3$ and $NH_3$ + $NH_2D$ + $NHD_2$ + $ND_3$ samples in selected regions are shown in Figures 3−5, respectively.

**Calculation Results.** Calculations were performed on three isomers of $MNH_3$, namely, the $MNH_3$ complexes, the inserted $HMNH_2$ molecules, and the $H_2MNH$ molecules on both singlet and triplet potential energy surfaces. The optimized structures are shown in Figure 6, and the vibrational frequencies and

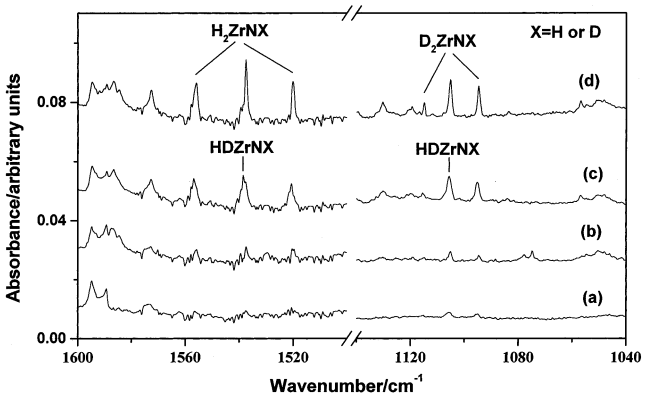


**Figure 5.** Infrared spectra in the 1600−1500 and 1140−1040 $cm^{-1}$ regions from codeposition of laser-ablated zirconium atoms with 0.4% ($NH_3$ + $NH_2D$ + $NHD_2$ + $ND_3$) in argon: (a) 1 h sample deposition at 11 K, (b) after 25 K annealing, (c) after 20 min broadband photolysis, and (d) after 28 K annealing.

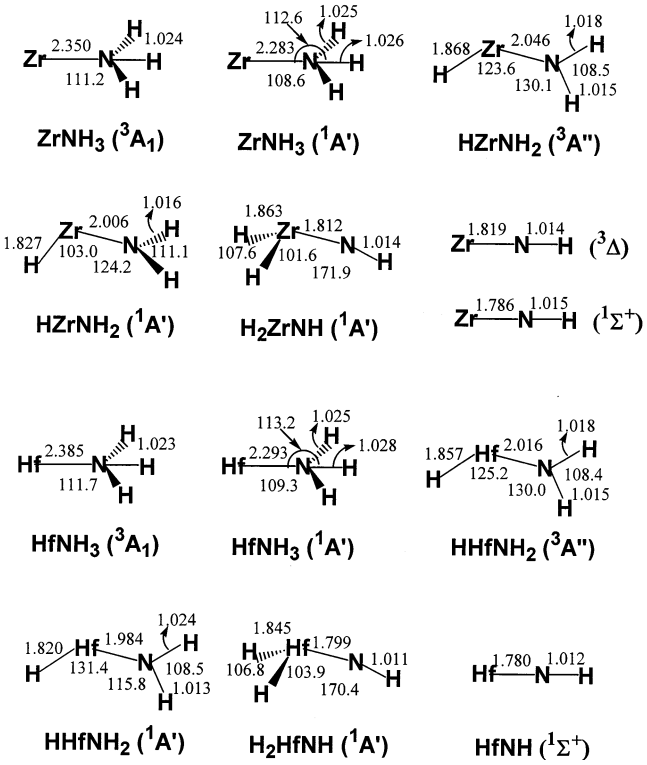


**Figure 6.** Calculated geometric parameters (bond length in angstrom, bond angle in degree) for the $ZrNH_3$ and $HfNH_3$ isomers and the ZrNH and HfNH molecules.

intensities are listed in Tables 2 and 3, respectively. Both the $ZrNH_3$ and $HfNH_3$ complexes have $^3A_1$ ground state with $C_{3v}$ symmetry. The $HZrNH_2$ molecule was predicted to have a $^3A''$ ground state with planar $C_s$ symmetry, and the $HHfNH_2$ molecule has a $^1A'$ ground state with planar $C_s$ symmetry. Both $H_2ZrNH$ and $H_2HfNH$ were predicted to have $^1A'$ ground state with nonplanar geometry. At the B3LYP level of theory, the $^1A'$ $H_2MNH$ molecule was predicted to be the most stable structure followed by the inserted $HMNH_2$ molecules.

**$MNH_3$.** A weak band at 1156.0 $cm^{-1}$ in the Zr + $NH_3$ experiments appeared on annealing but disappeared on broadband photolysis. It shifted to 1149.4 $cm^{-1}$ with $^{15}NH_3$ and gave an isotopic $^{14}N/^{15}N$ ratio of 1.0057. The band position and isotopic shift are characteristic of the symmetric bending vibration of perturbed $NH_3$ by interaction with one or more metal atoms. In the mixed $^{14}NH_3$ + $^{15}NH_3$ spectra, doublet isotopic structure was observed, which confirms that only one $NH_3$ unit is involved in this mode. The experiments employed quite low ablation laser energy to ensure that the matrix contained metal atoms to the virtual exclusion of metal clusters.

**TABLE 2: Calculated Vibrational Frequencies ($cm^{-1}$) and Intensities (km/mol) for the Reaction Intermediates, Products, and Various Transition States on the Potential Energy Surfaces of the Zr + $NH_3$ Reaction**

| molecule | frequency (intensity) |
|---|---|
| $ZrNH_3$ ($^3A_1$) | 3463.0 (25, e), 3350.4 (150, $a_1$), 1628.1 (22, e), 1208.9 (233, $a_1$), 463.5 (14, e), 318.1 (8, $a_1$) |
| $ZrNH_3$ ($^1A'$) | 3444.8 (3, a″), 3418.1 (4, a′), 3322.2 (161, a′), 1666.2 (34, a″), 1571.7 (10, a′), 1181.9 (335, a′), 470.1 (26, a″), 434.3 (8, a′), 355.4 (25, a′) |
| $HZrNH_2$ ($^3A''$) | 3590.2 (28, a′), 3492.8(28, a′), 1578.1 (424, a′), 1536.3 (43, a′), 632.5 (147, a′), 518.6 (15, a′), 510.1 (141, a″), 339.9 (28, a′), 225.9 (0.1, a′) |
| $HZrNH_2$ ($^1A'$) | 3599.4 (27, a″), 3501.5 (72, a′), 1678.0 (250, a′), 1478.2 (104, a′), 650.6 (66, a′), 496.1 (124, a′), 431.0 (36, a′), 363.4 (3, a″), 202.4 (6, a″) |
| $H_2ZrNH$ ($^1A'$) | 3592.0 (92, a′), 1637.1 (249, a′), 1598.0 (500, a″), 923.3 (189, a′), 603.9 (77, a′), 569.3 (284, a′), 540.1 (30, a′), 466.3 (148, a″), 440.6 (94, a′) |
| ZrNH ($^3\Delta$) | 3589.3 (75, $\sigma$), 900.4 (88, $\sigma$), 513.2 (222, $\pi$) |
| ZrNH ($^1\Sigma^+$) | 3580.3 (99, $\sigma$), 954.0 (67, $\sigma$), 590.0 (202, $\pi$) |
| TS1 | 3521.2 (35), 3434.3 (10), 1563.4 (69), 1387.5 (66), 831.3 (50), 789.8 (130), 525.0 (33), 470.4 (27), 1418.3i (1356) |
| TS2 | 3587.8 (27), 3482.5 (37), 1533.7 (162), 1422.4 (27), 784.2 (194), 710.5 (65), 493.8 (23), 210.3 (12), 1218.3i (913) |
| TS3 | 3601.6 (115), 1667.7 (148), 1625.6 (362), 942.5 (58), 812.4 (203), 589.0 (9), 491.3 (116), 440.1 (83), 1299.0i (1404) |
| TS4 | 3608.3 (104), 1947.8 (54), 1586.1 (128), 989.4 (15), 944.6 (2), 854.9 (106), 724.9 (101),430.2 (70), 1364.7i (525) |
| TS5 | 3607.8 (144), 1948.2 (102), 1674.4 (39), 1134.6 (10), 971.9 (6), 889.5 (89), 750.8 (74), 434.9 (62), 1291.9i (372) |

**TABLE 3: Calculated Vibrational Frequencies ($cm^{-1}$) and Intensities (km/mol) for the Reaction Intermediates, Products and Various Transition States on the Potential Energy Surfaces of the Hf + $NH_3$ Reaction**

| molecule | frequency (intensity) |
|---|---|
| $HfNH_3$ ($^3A_1$) | 3465.2 (46, e), 3358.4 (66, $a_1$), 1635.6 (25, e), 1218.7 (171, $a_1$), 457.1 (4, e), 246.1 (1, $a_1$) |
| $HfNH_3$ ($^1A'$) | 3469.3 (9, a″), 3343.5 (5, a′), 3265.0 (431, a′), 1680.0 (27, a″), 1492.3 (84, a′), 1199.4 (210, a′), 433.4(24, a″), 395.7(18, a′), 277.5(17, a′) |
| $HHfNH_2$ ($^3A''$) | 3593.4 (30, a′), 3497.4 (24, a′), 1610.6 (349, a′), 1540.4 (52, a′), 633.1 (105, a′), 513.1 (141, a″), 499.8 (8, a′), 325.1 (21, a′), 284.8 (6, a″) |
| $HHfNH_2$ ($^1A'$) | 3597.1 (60, a′), 3425.4(7, a′), 1683.4 (318, a′), 1541.9 (73, a′), 683.6 (73, a′), 577.5 (108, a″), 544.0 (1, a′), 356.2 (5, a′), 343.5 (4, a″) |
| $H_2HfNH$ ($^1A'$) | 3628.6 (90, a′), 1682.7 (204, a′), 1649.2 (380, a″), 921.5 (164, a′), 649.1 (96, a′), 607.8 (209, a′), 529.1 (193, a″), 478.4 (4, a″), 458.2 (118, a′) |
| HfNH ($^1\Sigma^+$) | 3628.3 (108, $\sigma$), 940.4 (51, $\sigma$), 582.6 (205, $\pi$) |
| TS1 | 3489.7 (33), 3411.9 (1), 1560.5 (47), 1409.8 (7), 820.4 (13), 790.3 (135), 480.8 (36), 473.0 (14), 1373.9i (1094) |
| TS2 | 3539.9 (35), 3430.7 (10), 1630.8 (135), 1487.7 (26), 971.5 (319), 615.5 (122), 438.1 (41), 358.8 (18), 931.7i (938) |
| TS3 | 3622.9 (103), 1687.4 (76), 1636.7 (352), 891.7 (55), 835.1 (155), 611.3 (15), 512.6 (128), 335.0 (83), 1271.0i (1369) |
| TS4 | 3633.1 (128), 1925.6 (52), 1609.6 (65), 1179.3 (9), 935.9 (5), 849.4 (114), 729.8 (68), 481.3 (81), 1406.5i (475) |

**TABLE 4: Scale Factors and Observed and Calculated Isotopic Frequency Ratios of the Observed Reaction Products**

| | | | $^{14}N/^{15}N$ | | H/D | |
|---|---|---|---|---|---|---|
| molecule | mode | scale factor | obsd | calcd | obsd | calcd |
| $ZrNH_3$ | $NH_3$ sym def | 0.956 | 1.0057 | 1.0057 | | 1.3055 |
| $HfNH_3$ | $NH_3$ sym def | 0.951 | 1.0051 | 1.0054 | | 1.3131 |
| $HZrNH_2$ | ZrH str | 0.937 | 1.0000 | 1.0000 | 1.3988 | 1.4058 |
| $H_2ZrNH$ | sym $ZrH_2$ str | 0.950 | 1.0000 | 1.0001 | 1.3956 | 1.4067 |
| | asym $ZrH_2$ str | 0.951 | 1.0001 | 1.0001 | 1.3888 | 1.4018 |
| | ZrNH str | 0.963 | 1.0262 | 1.0266 | | 1.0620 |
| $H_2HfNH$ | sym $HfH_2$ str | 0.959 | 1.0000 | 1.0001 | 1.3911 | 1.4095 |
| | asym $HfH_2$ str | 0.965 | 1.0000 | 1.0000 | 1.3947 | 1.4076 |
| | HfNH str | 0.975 | 1.0287 | 1.0286 | | 1.0409 |

It seems unlikely that this complex contains more than one metal atom. Accordingly, the 1156.0 $cm^{-1}$ band is assigned to the symmetric $NH_3$ bending vibration of the $ZrNH_3$ complex. With respect to the symmetric $NH_3$ bending vibration of matrix isolated $NH_3$ at 974.5 $cm^{-1}$,[35] the $ZrNH_3$ complex blue shifted 181.5 $cm^{-1}$, similar to those observed previously for the first row transition metal complexes.[18−21]

DFT calculation predicted that the $ZrNH_3$ complex has a $^3A_1$ ground state, with a symmetric $NH_3$ bending vibration of 1208.9 $cm^{-1}$. As listed in Table 4, the calculated $^{14}N/^{15}N$ ratio of 1.0057 is essentially the same with the experimental value. The N−H stretching and the antisymmetric $NH_3$ bending vibrational modes were predicted to be lower in intensity than the symmetric $NH_3$ bending mode and could not be observed in the experiments.

According to our DFT calculations, the $^3A_1$ ground state of $ZrNH_3$ has an electron configuration of $...(a_1)^2(e)^2$, which reflects the $4d^25s^2$ ground electron configuration of the Zr atom. The two metal-based electrons occupy a nonbonding $a_1$ molecular orbital, which is largely Zr 5s in character, and the remaining two electrons occupy the doubly degenerate e molecular orbitals, which are largely Zr 4d in character. The Zr−N bond length of ground-state $ZrNH_3$ was predicted to be 2.350 Å, slightly shorter than the value of 2.46 Å predicted by Siegbahn et al.[28] The binding energy with respect to ground-state Zr atom and free ammonia was estimated to be 20.3 kcal/mol, after zero point energy correction.

A similar band at 1158.8 $cm^{-1}$ in the Hf + $NH_3$ experiments is assigned to the symmetric $NH_3$ bending vibration of the $HfNH_3$ complex. The 1158.8 $cm^{-1}$ band was produced on 25 K annealing. It is extremely photosensitive. As demonstrated in Figure 2, the band intensity decreased markedly with increasing sample scan times, which implies that the red irradiation from the spectrometer can readily induce isomerization reaction of the $HfNH_3$ molecules. The $Hf^{15}NH_3$ absorption was observed at 1152.9 $cm^{-1}$. The $HfND_3$ counterpart could not be observed due to band overlap. The doublet absorptions in the mixed $^{14}NH_3 + {}^{15}NH_3$ isotopic experiments (Figure 4) verify the participation of one $NH_3$ unit in this molecule.

The $HfNH_3$ complex was also predicted to have a $^3A_1$ ground state. The ground state of $HfNH_3$ reflects the $5d^26s^2$ ground electron configuration of the Hf atom. The Hf−N bond length was predicted to be 2.385 Å. The binding energy with respect to ground state Hf atom and free ammonia was estimated to be 16.0 kcal/mol, slightly smaller than that of $ZrNH_3$. The calculated symmetric $NH_3$ bending vibration at 1218.7 $cm^{-1}$ and isotopic $^{14}N/^{15}N$ ratio of 1.0054 are in very good agreement with the experimental values.

**$HMNH_2$.** A weak band at 1478.4 $cm^{-1}$ in the Zr + $NH_3$ experiments appeared on annealing and increased on broadband photolysis. It exhibited no nitrogen-15 shift, but shifted to 1056.9 $cm^{-1}$ with $ND_3$, which defined a H/D ratio of 1.3988. This band is tentatively assigned to the Zr−H stretching vibration of the $HZrNH_2$ molecule. DFT calculations predicted this mode at 1578.1 $cm^{-1}$ and to be the most intense mode for the $^3A''$ ground-state $HZrNH_2$ molecule. The optimized geometric parameters and energy for the $HZrNH_2$ molecule is in quite good agreement with previous ab initio calculations.[28] No evidence was found for the $HHfNH_2$ molecule. DFT calculations indicated that the $HHfNH_2$ molecule has a $^1A'$ ground state with a strong Hf−H stretching vibration at 1683.4 $cm^{-1}$.

**$H_2MNH$.** In the Zr + $NH_3$ experiments, absorptions at 1556.0, 1520.3, 889.2, 887.8, and 886.4 $cm^{-1}$ can be grouped together by their consistent behavior upon annealing and photolysis. These bands were weak on sample deposition but were greatly enhanced on broadband photolysis when the $ZrNH_3$ absorption was eliminated. The increase upon photodestruction of $ZrNH_3$ implies that the new product is generated from $ZrNH_3$. The relative intensities of the 889.2, 887.8, and 886.4 $cm^{-1}$ absorptions matched the natural isotopic abundance of $^{90}Zr$, $^{92}Zr$, and $^{94}Zr$ ($^{90}Zr$, 51.4%; $^{92}Zr$, 17.1%; $^{94}Zr$, 17.5%) and clearly indicate that one zirconium atom is involved in this molecule. As shown in Figure 3, the 889.2, 887.8, and 886.4 $cm^{-1}$ bands shifted to 866.5, 865.0, and 863.5 $cm^{-1}$ with $^{15}NH_3$, and doublets were observed for these three bands in the mixed $^{14}NH_3 + {}^{15}NH_3$ experiment, which showed the participation of one nitrogen atom. The $^{14}N/^{15}N$ ratios (1.0262, 1.0264, and 1.0265) and the zirconium isotopic splitting imply that these three bands are due to a Zr−NH stretching vibration. The 1556.0 and 1520.3 $cm^{-1}$ bands exhibited no nitrogen-15 shift with the $^{15}NH_3$ sample, but they were shifted to 1114.9 and 1094.7 $cm^{-1}$ with $ND_3$ and gave isotopic H/D ratios of 1.3956 and 1.3888, respectively. The band positions and isotopic H/D ratios are close to the $ZrH_2$ stretching vibrations of the $H_2ZrO$ molecule (symmetric $ZrH_2$ stretching, 1577.7 $cm^{-1}$; H/D ratio, 1.3957; antisymmetric $ZrH_2$ stretching, 1539.4 $cm^{-1}$; H/D ratio, 1.3896),[36] which suggests that the 1556.0 and 1520.3 $cm^{-1}$ bands are due to $ZrH_2$ stretching vibrations. In the mixed $NH_3 + NH_2D + NHD_2 + ND_3$ experiment (spectra shown in Figure 5), two additional intermediate absorptions at 1537.5 and 1105.1 $cm^{-1}$ were produced besides pure isotopic counterparts, suggesting that two equivalent H atoms are involved in these two modes. Accordingly, we assign the 1556.0, 1520.3, and 889.2 $cm^{-1}$ bands to the symmetric and antisymmetric $ZrH_2$ stretching and Zr−NH stretching vibrations of the $H_2ZrNH$ molecule. The 1537.5 and 1105.1 $cm^{-1}$ bands in the mixed experiment are due to Zr−H and Zr−D stretching vibrations of the HDZrNH or HDZrND molecules.

The calculated frequencies at the optimized geometry of $H_2ZrNH$ provide excellent support for the proposed identification of this molecule. As has been mentioned, the $H_2ZrNH$ molecule was predicted to have a $^1A'$ ground state with $C_s$ symmetry. The symmetric and antisymmetric $ZrH_2$ stretching and the Zr−NH stretching modes were calculated at 1636.9, 1598.0, and 923.3 $cm^{-1}$, respectively, which require scale factors (observed value/calculated value) of 0.950, 0.951, and 0.963 to fit the experimental values. These three modes were predicted to be intense, with the antisymmetric $ZrH_2$ stretching mode to be the strongest (Table 2). Of particular important, the calculated isotopic frequency ratios for each mode are in excellent agreement with the experimental ratios (Table 4).

The 1614.7, 1590.9, and 898.3 $cm^{-1}$ absorptions in the Hf + $NH_3$ experiments are assigned to the $H_2HfNH$ molecule, following the example of $H_2ZrNH$. These three bands increased together at the expense of the $HfNH_3$ absorption, suggesting different vibrational modes of the same molecule that is

generated from $HfNH_3$. The 898.3 $cm^{-1}$ band went to 873.2 $cm^{-1}$ with $^{15}NH_3$, giving an isotopic $^{14}N/^{15}N$ ratio of 1.0287. The mixed $^{14}NH_3 + {}^{15}NH_3$ isotopic spectra (Figure 4) revealed only two isotopic bands and clearly indicates that only one N atom is involved in this mode. The band position and isotopic ratio are appropriate for a Hf−NH stretching vibration. The 1614.7 and 1590.9 $cm^{-1}$ bands showed no obvious nitrogen-15 shift with $^{15}NH_3$ sample, but gave deuterium counterparts at 1160.7 and 1140.7 $cm^{-1}$ and defined H/D ratios of 1.3911 and 1.3947, respectively. These H/D ratios are very close to the Hf−H stretching ratios of $HfH_x$ observed in solid argon,[37] suggesting that these two bands are due to Hf−H stretching vibrations. In the mixed $NH_3 + NH_2D + NHD_2 + ND_3$ experiment, two intermediate absorptions at 1606.0 and 1151.1 $cm^{-1}$ were produced, and these two bands are due to Hf−H and Hf−D stretching vibrations of the HDHfNH or HDHfND molecules.

Our DFT calculations on $H_2HfNH$ predicted that the molecule should be nonplanar and have a singlet ($^1A'$) ground state. The calculated symmetric and antisymmetric $HfH_2$ stretching and Hf−NH stretching vibrational frequencies, 1682.7, 1649.2, and 921.5 $cm^{-1}$, agree well with the experimental values (scale factors, 0.959, 0.965, and 0.975). Equally important, the calculated isotopic frequency ratios (Table 4) are in complete accord with the experimental values.

The $H_2ZrNH$ and $H_2HfNH$ molecules may be compared with the isoelectronic $H_2ZrO$ and $H_2HfO$ molecules recently reported.[36] The symmetric and antisymmetric $ZrH_2$ stretching and the Zr−NH stretching frequencies of $H_2ZrNH$ are lower than the symmetric and antisymmetric $ZrH_2$ stretching and the Zr−O stretching frequencies of $H_2ZrO$ by about 21.6, 19.1, and 35.5 $cm^{-1}$, respectively. These frequency separations between $H_2$-HfNH and $H_2HfO$ are estimated to be 31.7, 24.7, and 22.7 $cm^{-1}$. The Zr−N and Hf−N bond lengths were calculated to be 1.812 and 1.799 Å, respectively. The Zr−N and Hf−N approached triple bond in $H_2ZrNH$ and $H_2HfNH$.

In the Zr + $NH_3$/Ar experiments, two very weak bands at 1366.2 and 1320.2 $cm^{-1}$ were observed after sample deposition and were destroyed by full arc photolysis. Both bands exhibited very small nitrogen isotopic shifts (0.7 and 0.1 $cm^{-1}$). The deuterium counterparts were too weak to be observed. The photosensitive behavior suggests an anion species. These two bands are tentatively assigned to the symmetric and antisymmetric $ZrH_2$ stretching vibrations of $H_2ZrNH^-$. DFT calculations predicted $H_2ZrNH^-$ to have a $^2A'$ ground state with strong symmetric and antisymmetric $ZrH_2$ stretching vibrations at 1352.2 (439 km/mol) and 1308.0 $cm^{-1}$ (830 km/mol).

**Reaction Mechanism.** Although laser ablation of Zr and Hf targets produced ground state and excited metal atoms as well as ions in the gas phase, only ground-state metal atom reactions should be considered here, as the reactions proceeded in solid argon matrix after sample deposition. The spectra in Figures 1 and 2 clearly demonstrate that ground-state zirconium and hafnium atoms react with ammonia molecules in solid argon matrix to form metal−ammonia complexes: $ZrNH_3$ and $HfNH_3$. The $ZrNH_3$ and $HfNH_3$ absorptions increase on annealing, suggesting that reactions 1 and 2 require negligible activation energy.

$$Zr\ (^3F) + NH_3\ (^1A_1) \rightarrow ZrNH_3\ (^3A_1) \quad (1)$$

$$Hf\ (^3F) + NH_3\ (^1A_1) \rightarrow HfNH_3\ (^3A_1) \quad (2)$$

The absorptions due to the $ZrNH_3$ and $HfNH_3$ complexes disappeared on photolysis, during which the $HZrNH_2$, $H_2ZrNH$, and $H_2HfNH$ absorptions greatly enhanced, suggesting the photoinduced isomerism in reactions 3−5:

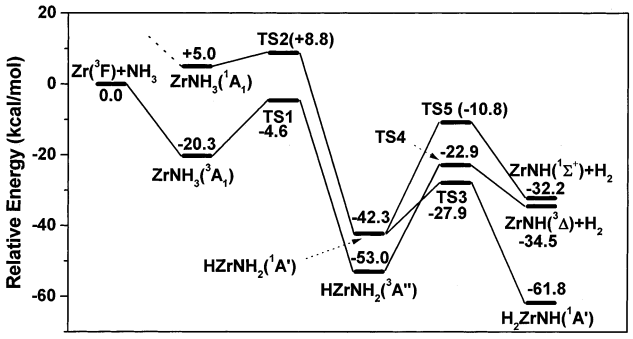


**Figure 7.** Potential energy surfaces following the reaction paths from Zr+$NH_3$, leading to the $H_2ZrNH$ and ZrNH + $H_2$ products. Energies given are in kcal/mol and are relative to the ground-state reactants: Zr ($^3F$) + $NH_3$ ($^1A_1$).

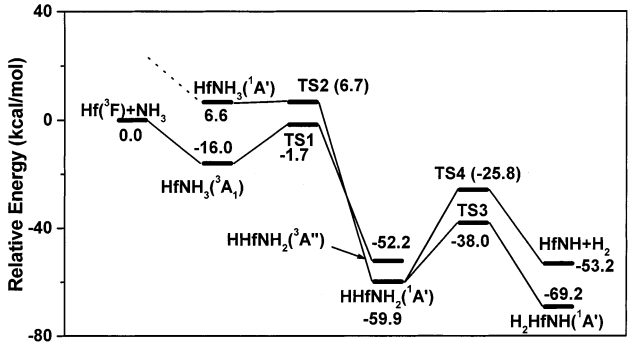


**Figure 8.** Potential energy surfaces following the reaction paths from Hf + $NH_3$, leading to the $H_2HfNH$ and HfNH + $H_2$ products. Energies given are in kcal/mol and are relative to the ground-state reactants: Hf ($^3F$) + $NH_3$ ($^1A_1$).

$$ZrNH_3\ (^3A_1) \rightarrow HZrNH_2\ (^3A'') \quad (3)$$

$$ZrNH_3\ (^3A_1) \rightarrow H_2ZrNH\ (^1A') \quad (4)$$

$$HfNH_3\ (^3A_1) \rightarrow H_2HfNH\ (^1A') \quad (5)$$

The DFT calculations suggested that the $HZrNH_2$ molecule is more stable than the $ZrNH_3$ complex by about 32.7 kcal/mol, while the $H_2ZrNH$ is more stable than the $ZrNH_3$ by about 41.5 kcal/mol. In the case of Hf, the $H_2HfNH$ molecule is predicted to be more stable than the $HfNH_3$ by as much as 53.2 kcal/mol.

Figures 7 and 8 show the singlet and triplet potential energy surfaces for the Zr + $NH_3$ and Hf + $NH_3$ reactions. The geometric parameters of the transition states on the potential energy surfaces are shown in Figure 9, and their vibratonal frequencies are listed in Tables 2 and 3. For both the Zr and Hf reaction systems, ground-state metal atoms interact with ammonia to form stable complexes. This initial step is exothermic and barrier free. From the complex, one hydrogen atom transfers from the nitrogen to the metal center to form the insertion intermediate. This isomerization process is also exothermic but proceeds through a transition state (TS1). In the case of Zr, both the $ZrNH_3$ complex and the $HZrNH_2$ insertion intermediate have a triplet ground state, and the transition state (TS1) lies about 4.6 kcal/mol lower than the ground-state reactants, Zr($^3F$) + $NH_3$, so the energy barrier from $ZrNH_3$ to $HZrNH_2$ was estimated to be 15.7 kcal/mol. The reaction process from $ZrNH_3$ to $HZrNH_2$ has also been theoretically studied by Siegbahn et

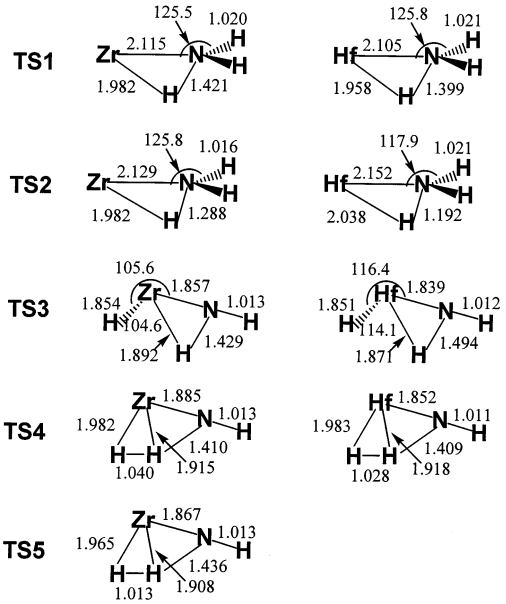


**Figure 9.** Calculated geometric parameters (bond length in angstrom, bond angle in degree) for the transition states on the potential energy surfaces shown in Figures 7 and 8.

al. using ab initio methods, and the transition state was predicted to lie 1 kcal/mol lower in energy than the ground-state reactants.[28] In the case of Hf, the $HfNH_3$ complex has a triplet ground state, but the $HHfNH_2$ has a singlet ground state. Formation of $HHfNH_2$ requires spin crossing, as shown in Figure 8. The transition state lies about 1.7 kcal/mol lower in energy than the ground-state reactants, $Hf(^3F) + NH_3$.

As shown in Figure 7, two reaction paths are possible starting from triplet ground-state $HZrNH_2$. One path is the $H_2$ elimination process to form $ZrNH + H_2$. This process is endothermic by about 18.5 kcal/mol with a 30.1 kcal/mol energy barrier. The other path is a second hydrogen atom transfer from nitrogen to the metal to form $H_2ZrNH$ via spin crossing. This process is predicted to be exothermic by about 8.8 kcal/mol with a 25.1 kcal/mol reaction energy barrier. In the case of Hf, the $HHfNH_2$, $H_2HfNH$, and HfNH molecules all have a singlet ground state, so the formation of both $H_2HfNH$ and HfNH from $HHfNH_2$ requires no spin crossing. The process from $HHfNH_2$ to $HfNH + H_2$ is endothermic by about 6.7 kcal/mol with an energy barrier of 34.1 kcal/mol, while the process from $HHfNH_2$ to $H_2HfNH$ is exothermic by about 9.3 kcal/mol with a 21.9 kcal/mol energy barrier. The path for the formation of $H_2HfNH$ is energetically favored over the $H_2$ elimination path.

It should be mentioned that weak $HZrNH_2$ absorption was observed in the $Zr + NH_3$ reaction, but no $HHfNH_2$ absorption was observed in the $Hf + NH_3$ reaction. Our theoretical calculation indicated that the reaction from complex to the inserted $HMNH_2$ molecule is highly exothermic for both metal systems. There is spin crossing from $HZrNH_2$ to $H_2ZrNH$, so part of the "hot" $HZrNH_2$ molecules probably have a chance to be stabilized by the matrix. However, there is no spin crossing from $HHfNH_2$ to $H_2HfNH$, and this may suggest that $HHfNH_2$ is very short-lived, rapidly rearranging to form the $H_2HfNH$ molecule.

The results for zirconium and hafnium atom and ammonia reactions are quite similar with the metal atom and water reactions.[37] The main difference is the formation of stable complexes in the metal atom and ammonia reactions compared to the corresponding water reactions. In the water reaction, there is no evidence of the metal−water complex, and the HZrOH, $H_2ZrO$, and $H_2HfO$ molecules produced spontaneously on annealing.[36] Ammonia and water are isoelectronic molecules. The difference is that water has two lone pair electrons while ammonia has only one and that the lone pairs of water are more tightly bound than that in ammonia. As has been discussed,[38] the more diffuse lone pair of ammonia is the origin of the larger binding energies for the complexes than that of water.

The reactions of Zr and Hf with $NH_3$ are different than the reactions of Sc and Y with $NH_3$. In the cases of Sc and Y, both gas phase[16,17] and matrix isolation[21] investigations indicated that the final reaction products are $ScNH + H_2$ and $YNH + H_2$. As has been discussed,[21] the reaction difference is a direct consequence of the change in valence electron configurations of the metal atoms. Sc and Y have only three valence electrons; there are not enough electrons to satisfy chemical bonding in forming $H_2ScNH$ and $H_2YNH$, so the $H_2$ elimination process is the major reaction path. Zr and Hf have four valence electrons to satisfy the chemical bonding in forming $H_2ZrNH$ and $H_2HfNH$, and the dominant reaction process is the formation of energetically favored $H_2ZrNH$ and $H_2HfNH$.

## Conclusions

Reactions of zirconium and hafnium atoms with ammonia molecules in solid argon matrix have been studied by infrared absorption spectroscopy and density functional theoretical calculations. The metal atoms were produced by pulsed laser ablation of pure metal targets. Various reaction intermediates and their photolysis products have been produced and identified by isotopic substitutions as well as density functional theoretical frequency calculations.

The ground-state zirconium and hafnium atoms reacted with ammonia to form the $ZrNH_3$ and $HfNH_3$ complexes spontaneously on annealing in solid argon. Density functional calculations showed that these complexes have triplet ground state with $C_{3v}$ symmetry and are correlated with the $d^2s^2$ electron configurations of the metal atoms. Near UV or visible light photolyses bring about photochemical rearrangement of the $ZrNH_3$ and $HfNH_3$ complexes with the insertion of the metal atoms into the N−H bonds of ammonia to form the planar $HZrNH_2$ and finally to the nonplanar $H_2ZrNH$ and $H_2HfNH$ molecules. These photoisomerism reactions are exothermic and proceed via transition states.

The results on metal atom and ammonia reactions have been compared with the metal atom and water reactions. As ammonia and water are isoelectronic molecules, we find that the reaction mechanisms are similar, and the main difference is the formation of stable complexes in the metal atom and ammonia reactions compared to the corresponding water reactions.

**Acknowledgment.** We gratefully acknowledge financial support from NSFC (Grant 20003003 and 20125033), the NKBRSF of China, and ammonia gas from Dr. Shirun Yan.

## References and Notes

(1) See, for examples: Macgregor, S. A. *Organometallics* **2001**, *20*, 1860; Müller, T. E.; Beller, M. *Chem. Rev.* **1998**, *98*, 675; Roundhill, D. M. *Chem. Rev.* **1992**, *92*, 1; Casalnuovo, A. L.; Calabrese, J. C.; Milstein, D. *Inorg. Chem.* **1987**, *26*, 971; Koelliker, R.; Milstein, D. *J. Am. Chem. Soc.* **1991**, *113*, 8524.

(2) Buckner, S. W.; Gord, J. R.; Freiser, B. S. *J. Am. Chem. Soc.* **1988**, *110*, 6606.

(3) Guo, B. C.; Kerns, K. P.; Castleman, A. W., Jr. *J. Phys. Chem.* **1992**, *96*, 4879; MacTaylor, R. S.; Vann, W. D.; Castleman, A. W., Jr. *J. Phys. Chem.* **1996**, *100*, 5329.

(4) Kaya, T.; Kobayashi, M.; Shinohara, H.; Sato, H. *Chem. Phys. Lett.* **1991**, *186*, 431; Sato, H. *Res. Chem. Intermed.* **1993**, *19*, 67.

(5) Clemmer, D. E.; Sunderlin, L. S.; Armentrout, P. B. *J. Phys. Chem.* **1990**, *94*, 208; Clemmer, D. E.; Sunderlin, L. S.; Armentrout, P. B. *J. Phys. Chem*. **1990**, *94*, 3008.

(6) Kooi, S. E.; Castleman, A. W., Jr. *Chem. Phys. Lett*. **1999**, *315*, 49.

(7) Marridis, A.; Herrera, F. L.; Harrison, J. F. *J. Phys. Chem.* **1991**, *95*, 6854.

(8) Russo, N.; Sicilia, E. *J. Am. Chem. Soc.* **2001**, *123*, 2588; Ye, S. *Theochem.* **1995**, *357*, 147.

(9) Clemmer, D. E.; Armentrout, P. B. *J. Am. Chem. Soc.* **1989**, *111*, 8280.

(10) Hendrickx, M.; Ceulemans, M.; Gong, K.; Vanquickenborne, L. *J. Phys. Chem. A* **1997**, *101*, 8540.

(11) Nakao, Y.; Taketsugu, T.; Hirao, K. *J. Chem. Phys.* **1999**, *110*, 10863.

(12) Marinelli, P. J.; Squires, R. R. *J. Am. Chem. Soc*. **1989**, *111*, 4101.

(13) Walter, D.; Armentrout, P. B. *J. Am. Chem. Soc*. **1998**, *120*, 3176.

(14) Bauschlicher, C. W., Jr.; Langhoff, S. R.; Partridge, H. *J. Chem. Phys.* **1991**, *94*, 2068; Langhoff, S. R.; Bauschlicher, C. W., Jr.; Partridge, H.; Sodupe, M. *J. Phys. Chem.* **1991**, *95*, 10677.

(15) Magnusson, E.; Moriarty, N. W. *Inorg. Chem*. **1996**, *35*, 5711.

(16) Steimle, T. C.; Xin, J.; Marr, A. J.; Beaton, S. *J. Chem. Phys.* **1997**, *106*, 9084.

(17) Jakubek, Z. J.; Simard, B.; Niki, H.; Balfour, W. J. *J. Chem. Phys*. **1999**, 111, 1483; **2000**, *113*, 3591. Simard, B.; Balfour, W. J.; Vasseur, M.; Hackett, P. A. *J. Chem. Phys.* **1990**, *93*, 4481.

(18) Kauffman, J. W.; Hauge, R. H.; Margrave, J. L. *High. Temp. Sci*. **1984**, *17*, 237.

(19) Szczepanski, J.; Szczesniak, M.; Vala, M. *Chem. Phys. Lett*. **1989**, *162*, 123.

(20) Ball, D. W.; Hauge, R. H.; Margrave, J. L. *High. Temp. Sci*., **1988**, *25*, 95; Ball, D. W.; Hauge, R. H.; Margrave, J. L. *Inorg. Chem*. **1989**, *28*, 1599.

(21) Chen, M. H.; Lu, H.; Dong, J.; Miao, L.; Zhou, M. F. In press.

(22) Bauschlicher, C. W., Jr. *J. Chem. Phys.* **1986**, *84*, 260.

(23) Papai, I. *J. Chem. Phys.* **1995**, *103*, 1850.

(24) Fournier, R. *J. Chem. Phys.* **1995**, *102*, 5396; Chan, W. T.; Fournier, R. *Chem. Phys. Lett.* **1999**, *315*, 257.

(25) Tsipis, A. C. *J. Chem. Soc., Faraday Trans*. **1998**, *94*, 11.

(26) Jackson, K. A.; Knickelbein, M.; Koretsky, G.; Srinivas, S. *Chem. Phys*. **2000**, *262*, 41.

(27) Lacaze-Dufaure, C.; Mineva, T.; Russo, N. *J. Comput. Chem*. **2001**, *22*, 1557.

(28) Blomberg, M. R. A.; Siegbahn, P. E. M.; Svensson, M. *Inorg. Chem.* **1993**, *32*, 4218.

(29) Chen, M. H.; Wang, X. F.; Zhang, L. N.; Yu, M.; Qin, Q. Z. *Chem. Phys*. **1999**, *242*, 81; Zhou, M. F.; Zhang, L. N.; Qin, Q. Z. *J. Am. Chem. Soc.* **2000**, *122*, 4483.

(30) Frisch, M. J.; Trucks, G. W.; Schlegel, H. B.; Scuseria, G. E.; Robb, M. A.; Cheeseman, J. R.; Zakrzewski, V. G.; Montgomery, Jr., J. A.; Stratmann, R. E.; Burant, J. C.; Dapprich, S.; Millam, J. M.; Daniels, A. D.; Kudin, K. N.; Strain, M. C.; Farkas, O.; Tomasi, J.; Barone, V.; Cossi, M.; Cammi, R.; Mennucci, B.; Pomelli, C.; Adamo, C.; Clifford, S.; Ochterski, J.; Petersson, G. A.; Ayala, P. Y.; Cui, Q.; Morokuma, K.; Malick, D. K.; Rabuck, A. D.; Raghavachari, K.; Foresman, J. B.; Cioslowski, J.; Ortiz, J. V.; Baboul, A. G.; Stefanov, B. B.; Liu, G.; Liashenko, A.; Piskorz, P.; Komaromi, I.; Gomperts, R.; Martin, R. L.; Fox, D. J.; Keith, T.; Al-Laham, M. A.; Peng, C. Y.; Nanayakkara, A.; Gonzalez, C.; Challacombe, M.; Gill, P. M. W.; Johnson, B.; Chen, W.; Wong, M. W.; Andres, J. L.; Gonzalez, C.; Head-Gordon, M.; Replogle, E. S.; Pople, J. A. *Gaussian 98*, Revision A.7, Gaussian, Inc.: Pittsburgh, PA, 1998.

(31) Becke, A. D. *J. Chem. Phys.* **1993**, *98*, 5648; Lee, C.; Yang, E.; Parr, R. G. *Phys. Rev. B* **1988**, *37*, 785.

(32) Wadt, W. R.; Hay, P. J. *J. Chem. Phys.* **1985**, *82*, 284; Hay, P. J.; Wadt, W. R. *J. Chem. Phys.* **1985**, *82*, 299.

(33) See for examples: Wittborn, A. M. C.; Costas, M.; Blomberg, M. R. A.; Siegbahn, P. E. M. *J. Chem. Phys.* **1997**, *107*, 4318; Bytheway, I.; Wong, M. W. *Chem. Phys. Lett.* **1998**, *282*, 219; Frenking, G.; Frohlich, N. *Chem. Rev.* **2000**, *100*, 717.

(34) Peng, C.; Ayala, P. Y.; Schlegel, H. B.; Frisch, M. J. *J. Comput. Chem.* **1996**, *17*, 49.

(35) Suzer, S.; Andrews, L. *J. Chem. Phys*. **1987**, *87*, 5131.

(36) Zhou, M. F.; Zhang, L. N.; Dong, J.; Qin, Q. Z. *J. Am. Chem. Soc.* **2000**, *122*, 10680.

(37) Chertihin, G. V.; Andrews, L. *J. Phys. Chem.* **1995**, *99*, 15004.

(38) Siegbahn, P. E. M.; Blomberg, M. R. A.; Svensson, M. *J. Phys. Chem.* **1993**, *97*, 2564.